Light Scattering Measurements of Subcellular Structure Provide Noninvasive Early Detection of Chemotherapy-induced Apoptosis[1]

Kevin J. Chalut[*], **Julie Hanson Ostrander**[*], **Michael G. Giacomelli**, and **Adam Wax**[2]
Department of Biomedical Engineering, Fitzpatrick Institute for Photonics, Duke University, Durham, North Carolina 27708 [KJC, MGG, AW]; Department of Medicine, Division of Medical Oncology, Duke University Medical Center, Durham, NC 27710 [JHO]

Abstract

We present a light scattering study using angle-resolved low coherence interferometry (a/LCI) to assess nuclear morphology and sub-cellular structure within MCF-7 cells at several timepoints following treatment with chemotherapeutic agents. While the nuclear diameter and eccentricity are not observed to change, the light scattering signal reveals a change in the organization of sub-cellular structures that we interpret using fractal dimension (FD). The FD of sub-cellular structures in cells treated with paclitaxel and doxorubicin is observed to increase significantly compared to that of control cells as early as 1.5 and 3 hrs after application, respectively. The FD is then found to decrease slightly at 6 hrs post application for both agents only to increase again from 12 to 24 hrs post treatment when the observations ceased. The changes in structure appear over two time scales, suggesting that multiple mechanisms are evident in these early apoptotic stages. Indeed, quantitative image analysis of fluorescence micrographs of cells undergoing apoptosis verify that the FD of DAPI stained nuclear structures does not change significantly in cells until 12 hrs after treatment while that of MitoTracker stained mitochondria is seen to modulate as early as 3 hrs after treatment. In contrast, cells receiving an increased dose of paclitaxel that induced G2/M arrest, but not apoptosis, only exhibited the early change in sub-cellular structure but did not show the later change associated with changes in nuclear substructure. These results suggest the a/LCI may have utility in detecting early apoptotic events for both clinical and basic science applications.

Keywords

a/LCI; light scattering; apoptosis; paclitaxel; doxorubicin

Introduction

Dysregulation of programmed cell death, apoptosis, has important implications in normal development and disease. A key step in cancer initiation and progression is escape from normal apoptotic controls that lead to the elimination of cancer cells (1). In addition, defective apoptotic signaling results in cancer cells that may be resistant to, or become resistant to, chemotherapeutic treatments. Extensive research has been done and is currently underway to

[2] To whom requests for reprints should be addressed, at Department of Biomedical Engineering, Box 90281, Duke University, Durham, NC 27708. Phone: (919) 660−5143; Fax: (919) 684−4488; E-Mail: a.wax@duke.edu.
[*]Authors contributed equally to this work.

understand apoptotic signaling pathways and how these pathways are perturbed in cancer and other diseases (2). Additional efforts are being put forth to develop technologies to detect apoptosis *in vivo* (3). Non-invasive *in vivo* detection of apoptosis has great potential to enhance our ability to monitor patients undergoing cancer therapy and could provide rapid feedback on whether a patient is responding to current conventional therapies or newly developed drugs. Currently, many non-invasive imaging techniques require radioactive labels and contrast agents (3). We aim to develop an optical technology that uses endogenous contrast to detect early structural changes characteristic of apoptosis.

Two distinct modes of apoptosis have been described, extrinsic and intrinsic. Extrinsic activation of apoptosis is dependent on activation of death receptors (i.e. TNFR family), while intrinsic apoptosis activation results from disruption of intracellular homeostasis (DNA damage, cellular stress). Taxanes and anthracylines, such as paclitaxel and doxorubicin, respectively, are used to treat a variety of types of cancer and lead to the activation of intrinsic apoptotic pathways. Paclitaxel enhances microtubule stability, resulting in G2/M arrest and apoptosis. Doxorubicin is a topoisomerase II inhibitor and inhibits DNA and RNA synthesis. While these two chemotherapy agents have different mechanisms of action, both have been shown to induce apoptosis in MCF-7 breast cancer cells (4,5). We aim to determine if similar changes in sub-cellular structure following drug treatment can be detected using light scattering methods.

Intrinsic and extrinsic apoptosis both result in a highly ordered apoptotic process that is characterized by specific morphological and biochemical changes. Morphological changes include chromatin condensation, cell shrinkage and membrane blebbing (2). Common biochemical events include translocation of phosphotidylserine to the outer plasma membrane, caspase activation, and DNA fragmentation (2). These common morphological and biochemical characteristics have directed the study of molecular events associated with apoptosis and resistance to apoptotic stimuli. For example, there are numerous assays available to identify DNA fragmentation, an end result of apoptosis. These include flow cytometry approaches in which DNA from fixed cells is labeled with an exogenous dye, such as propidium iodide, DAPI, or Hoescht, and then cellular DNA content is examined on a cell by cell basis (6). Additionally, there are assays for caspase activation, which involve incubating live cells or a cellular lysate with a caspase cleavage site conjugated to an exogenous fluorophore (chromophore) that fluoresces (absorbs) once cleaved (7). Assays that differentiate early and late apoptotic events use Annexin V fluorescent conjugates, which bind to the exposed phosphotidylserine, in combination with dyes (i.e. propiduim iodide, 7-AAD) that only enter cells following loss of membrane integrity (6). While more recent data indicates that additional subcellular structural and functional changes commonly occur during early apoptosis (8-10), techniques that provide early, noninvasive detection of apoptosis have been previously unavailable.

In the present study, we applied angle-resolved low coherence interferometry (a/LCI) (11, 12), a noninvasive light scattering technique that is highly sensitive to changes in subcellular structure, to the study of apoptosis in MCF-7 breast cancer cells. The a/LCI technique provides an alternative to imaging for probing subcellular morphology. With this method, the change in momentum of photons due to interaction with a sample is examined to quantitatively probe its structure (13). The main advantage of a/LCI is that it is a non-perturbative optical modality, i.e. it uses light in the spectral region known as the 'therapeutic window' for optical imaging (near infrared wavelengths) (14). The optical therapeutic window is especially important for *in vivo* diagnostic techniques, because major tissue chromophores, such as water, hemoglobin, and melanin, do not absorb light at these wavelengths. We show that, by using a/LCI to measure the fractal dimension (FD) of structures within MCF-7 cells treated with paclitaxel and

doxorubicin, we can sensitively distinguish between control cells and cells undergoing apoptosis within three hours of treatment.

The a/LCI method has been developed to detect neoplasia in animal models by measuring changes in nuclear morphology (15,16) and, more recently, has been applied to assess nuclear deformation in studies of cellular response to environmental stimuli (17). A/LCI and other light scattering techniques have demonstrated the ability to assess FD in biological samples (13, 15,18,19). Moreover, light scattering techniques, including a/LCI, have been used to assess apoptosis *in vivo* (15) and in cell studies (20-23). The present study extends this previous work by sensitively detecting early changes in response to apoptosis-inducing chemotherapeutic drugs. Additionally, the present study points to fractal dimension as an important indicator of structural changes in cells specifically related to apoptosis. Finally, mechanisms for structural changes that affect the fractal dimension are quantified and explored in order to better understand the rubric of fractal dimension and its potential for indicating apoptosis.

Materials and Methods

Angle-resolved low coherence interferometry (a/LCI)

a/LCI, which is outlined in detail in references (11,12), obtains depth-resolved measurements of the far-field diffraction of a biological sample, which corresponds to a cell monolayer in the present study. Low coherence interferometry permits the rejection of multiply scattered light that can cause noise artifacts in the signal. The signal resulting from an a/LCI measurement is processed to isolate the scattering from individual cell nuclei and all smaller organelles in the ensemble while eliminating contributions from long range correlations within the monolayer (24). The processed nuclear scattering profile is then analyzed using an inverse light scattering analysis (ILSA) algorithm to determine the properties of the nucleus (shape, size, etc.). Traditional ILSA algorithms for analyzing scattering from biological samples have generally used Mie theory, a model of spherical scatterers; however, in the present study, the ILSA algorithm uses a T-matrix light scattering model (25), which predicts scattering from spheroidal scatterers. The T matrix-based ILSA algorithm has been shown to yield accurate measurements of the average equal volume diameter, EVD, and the average aspect ratio, ε, of stretched microspheres in tissue phantoms (26) and cell nuclei in monolayers (27).

The predicted nuclear scattering profile can now be subtracted from the original data, which comprises nuclear scattering plus scattering due to smaller organelles, to isolate the slowly varying background in the scattering signal which corresponds to smaller organelles (smaller than ~2 μm). This residual scattering signal is Fourier transformed to yield the two-point density correlation function of small organelles, which generally exhibits a power law function. Density correlations that obey a power law indicate self-similarity in a distribution (28); in the cellular materials investigated in the present study, the power law form held over 1−2 orders of magnitude of size scale (13). The exponent of the power law can be physically interpreted as representing a mass fractal in three dimensions, and can be used to deduce the mass fractal dimension (mass FD).

The T matrix database used for the ILSA algorithm computed scattering from spheroidal particles with EVD ranging from 7.8 to 12.2 μm, ε ranging from 0.56 to 0.9, size distributions of 7% and 10%, background index of refraction from 1.35 to 1.36, and scattering refractive index from 1.42 to 1.43. These ranges of values are based on quantitative image analysis of MCF-7 cell samples and published values for cellular refractive indices (29). A least-squares fitting of the processed scattering data was utilized in the ILSA algorithm to determine the most probable scattering configuration from the database. For more extensive details concerning a/LCI optics, processing of the a/LCI signal, the ILSA algorithm, and the statistical techniques, please see supplemental methods.

Cell culture

MCF-7 breast cancer cells, obtained from the Duke University Cell Culture facility, were maintained in minimal essential medium alpha (Invitrogen), supplemented with 5% FBS, 10 mM HEPES (Invitrogen), 1x non-essential amino acids (Invitrogen), 1x sodium pyruvate (Invitrogen), 1 μg/mL insulin (Invitrogen), 1 μg/mL hydrocortisone (sigma), and 10 ng/mL EGF (sigma). For a/LCI measurements, MCF-7 cells were plated at 2.5×10^5 cells/well in 2-well chamber slides and incubated over night at 37°C, 5% CO_2. For all treated samples 5 or 50 nM paclitaxel (sigma), or 5 μM doxorubicin (EMD biosciences) was added to growth medium and then the cellular medium was replaced. The medium for the control (untreated) cells was changed at the beginning of the experiment as well.

Flow Cytometry

MCF-7 cells were plated at 2.5×10^5 cells/well in 6-well plates and treated in triplicate with either vehicle control (DMSO), 5 nM , or 50 nM paclitaxel for indicated times. Cell were trypsinized, pelleted by centrifugation, and then fixed with 80% ethanol. Samples were placed at −20 °C until the day of analysis. On the day of analysis, cell pellets were washed twice with PBS and then resuspended in 300 μl of fluorescence-activated cell sorting buffer (1.37 M NaCl, 27 mM KCl, 43 mM Na_2HPO_4, 14.7 mM KH_2PO_4, 1 mg/mL ribonuclease A, 0.5 mM EDTA, 0.1% Triton X-100 and 0.2 mg/ml propidium iodide). Samples were analyzed by the Duke University Flow Cytometry facility for DNA content.

Quantitative image analysis (QIA)

MCF-7 cells were plated at 1×10^5 cells/well in 4-well chamber slides and treated as described above. All treatment groups were fixed in 4% paraformaldehyde and nuclei were stained with 4,6-diamidino-2-phenylindole (DAPI) (Sigma Aldrich). Samples were thoroughly washed with PBS and mounted onto glass cover slips with Vectashield (Vector Laboratories, Ashland, MA) before images were obtained with fluorescence microscopy (Figure 4a and 4b). Each sample was imaged (40x) at 3−4 separate regions at T = 3, 6, 12, and 24 hours. These images were analyzed using ImageJ NIH image processing software (Bethesda, MD). Reported nuclear diameters are based on size determinations for n = 70 cells. To compute box counting fractal dimension (box FD), distinct cell nuclei were individually isolated and analyzed for a total of ~40 cell nuclei for each post-treatment time point. Each isolated nucleus was converted to a binary image and the box FD was computed using the builtin fractal dimension function in ImageJ. Box sizes of 2,3,4,6,8,12,16,32,64 pixels were used. An important distinction exists between the box FD, which is computed from 2D images, and the mass FD, which is computed from the a/LCI data as a 3D mass fractal (13). At all times in the text, FD as computed by QIA will be referred to as box FD, and FD as computed by a/LCI will be referred to as mass FD.

For MitoTracker experiments, MCF-7 cells were plated at 2.5×10^5 cells/dish in 35 mm glass bottom dishes (MatTek) and incubated overnight at 37°C, 5% CO_2. The following day, MCF-7 cells were treated with 5 nM paclitaxel for 3, 6, and 12 hours. For control samples, the growth medium was changed and cells were incubated in parallel to paclitaxel treated samples. 1 hour prior to imaging 100 nM MitoTracker FM Green was added to all samples. MitoTracker images were acquired using a Leica SP5 confocal microscope (Duke University Light Microscopy Core Facility). MitoTracker FM Green was excited at 488 nm and emission spectra were collected from 510−580 nm. 3−4 images were taken per plate, 2 plates per treatment group, per time point with a 40×/1.25 Oil objective (Figure 4c and 4d). The box FD was computed as described above on a per cell basis (n ≥ 40).

Statistical methods—All *p*-values were calculated by using a rank sum test in Matlab (Mathworks, Natick, MA) using the default value of α = 0.05.

Results

Paclitaxel induces apoptosis and G2/M arrest in MCF-7 cells

To determine the optimal concentration of paclitaxel to induce apoptosis in MCF-7 cells, cells were treated with increasing concentrations of paclitaxel (0, 1, 5, 10, 25 and 50 nM) for 24 hours. Cells were fixed and stained with propidium iodide. Flow cytometry cell cycle analysis showed that compared to control cells (6.48 ±1.23%), 1 and 5 nM concentrations of paclitaxel induced a significant increase in the percentage of cells with a sub-G1 content of DNA, 18.26 ±1.27% and 21.03 ±2.55%, respectively (Figure 1). Further, higher concentrations of paclitaxel (10, 25, and 50 nM), only induced an increase in cells arrested in G2/M and not apoptosis (Figure 1). To determine the optimal time of exposure, MCF-7 cells were either left untreated or treated with 5 nM paclitaxel for 3, 6, 9 and 24 hours and fixed and stained with propidium iodide for cell cycle analysis. As shown in Figure 2, 5 nM paclitaxel induced a significant increase in cells with sub-G1 content of DNA within 6 hours, 3.0 ±0.42 in control cells to 5.07 ±0.25 in paclitaxel treated cells. By 24 hours approximately 30% of the paclitaxel-treated cells were apoptotic. A similar set of experiments were performed with doxorubicin. We determined that the optimal concentration of doxorubicin to induce apoptosis in MCF-7 cells was 5 μM, and, similar to paclitaxel treated MCF-7 cells, an increase in apoptotic cells was observed within 6 hours of treatment (data not shown).

a/LCI fractal dimension

Using T-matrix theory-based ILSA, the size and shape of the MCF-7 cell nuclei (EVD) was found to agree with the results of QIA of DAPI-stained samples to a high degree of accuracy (supplementary Fig. S3). We found no significant changes in nucleus EVD or aspect ratio for treated or control cells throughout the observation window, using either the a/LCI technique or QIA.

No discernible pattern was observed for the mass FD of the paclitaxel-treated MCF-7 cells when using Mie theory-based ILSA (supplementary Fig. S2). Therefore, the T matrix-based ILSA algorithm described above was instead used to determine the mass FD of control MCF-7 cells and cells treated with 5 nM paclitaxel. These results demonstrate an increase in mass FD from $D = 1.63 \pm 0.44$ (in the form of mean $\pm$ SD) to $D = 2.13 \pm 0.13$ from t = 0 to 3 h, but then regressed slightly at t = 6 h to 1.95 ± 0.17. The mass FD increased to 2.00 ± 0.24 and 2.02 ± 0.14 at 12 and 24 hours, respectively. The mass FD of control cells ranges from 1.50 to 1.70 with SD ranging from 0.20 to 0.40. The mass FD of treated cells at t = 3, 12, and 24 h shows statistically significant differences from both control cells and treated cells at t = 0 h. The difference between the mass FD of treated cells at t = 6 h and control cells at the same time point are also statistically significant but at this timepoint, there is no statistical significance between treated cells at t=0. All results from treated and control groups are shown in Figure 3a, which also indicates where results are statistically significant.

To determine if the paclitaxel-induced changes in FD are specific to taxane-based chemotherapy treatments, MCF-7 cells were treated with doxorubicin, an anthracyline which inhibits topoisomerase II and inhibits DNA and RNA synthesis. MCF-7 cells were either left untreated (control) or treated with doxorubicin for 3, 6, 12 and 24 hours. In doxorubicin-treated MCF-7 cells, the mass FD increased from $D = 1.76 \pm 0.17$ at t = 0 h to $D = 1.98 \pm 0.21$ at t = 3 h and then regressed slightly to $D = 1.92 \pm 0.21$ at t = 6 h. The mass FD increased to 2.00 ± 0.16 at t = 12 h and to 2.06 ± 0.09 at 24 h. The mass FD of control cells range from 1.50 to 1.75 with SDs ranging from 0.15 to 0.40. The mass FD of treated cells at t = 3, 12, and 24 h represents statistically significant differences from control cells and treated cells at t = 0 h (Figure 3b) with again no statistically significant differences seen between the t = 0h and the t = 6 h timepoint

To investigate if changes could be detected at earlier time points, MCF-7 cells were treated with 5 nM paclitaxel and compared to control cells at t = 1.5 h post treatment. The T matrix-based ILSA algorithm determines the mass FD to be D = 2.05 ± 0.20 at this time point, compared with D = 1.59 ± 0.26 for the control cells, a statistically significant difference (p<0.05). The mass FD of treated cells at t = 1.5 h represents a highly statistically significant difference from control cells and treated cells at t = 0 h (Figure 3c).

MCF-7 cells treated with 50 nM paclitaxel arrest in the G2/M phase of the cell cycle (Figure 1). Therefore, to determine if the a/LCI mass FD results are indicative of apoptosis, MCF-7 cells were either left control or treated with 50 nM paclitaxel for 3, 6, 12 and 24 hours (supplementary Fig. S5). Interestingly, there is a significant difference between the mass FD of treated cells and control cells at t = 3 h, after which point the mass FD recovered to the same as control cells; no statistically significant differences exist beyond 3 h.

QIA box counting fractal dimension of cell nuclei

The box FD was computed by QIA of images (Figure 4a and 4b) taken from DAPI-stained MCF-7 cells either left untreated or treated with 5 nM paclitaxel. The FD of treated cells increased from 1.62 ± 0.08 at t = 3 h to 1.64 ± 0.05 at t = 6 h to 1.71 ± 0.08 at t = 12 h and t = 24 h. The box FD of control cells was between 1.60 and 1.62 with a SD of 0.05 at all time points. The differences between FD of treated and control cells are statistically significant at t = 12 and 24 h. See Figure 5a for a summary of results.

QIA box counting fractal dimension of mitochondria

The box FD was computed by QIA of images (Figure 4c and 4d) taken from MitoTracker FM Green-stained MCF-7 cells treated with 5 nM paclitaxel and control samples. The box FD of treated cells at t = 3 h was 1.65 ± 0.07 while the FD of control cells at t = 3 h was 1.60 ± 0.06. The box FD of treated cells at t = 6 h was 1.60 ± 0.08 while the box FD of control cells at t = 6 h was 1.56 ± 0.08. Finally, the box FD of treated cells at t = 12 h was 1.63 ± 0.06 while the box FD of control cells at t = 12 h was 1.59 ± 0.07. At each time point, the difference in box FD between treated and control cells is statistically significant (p < 0.05), and the difference at t = 3 h and t = 12 h is highly significant (p < 0.001). See Figure 5b for summary of results.

Discussion

Fractal dimension is a measure of the texture of an object: as a mass distribution transitions from a fine, smooth structure to a coarser, grainer structure, the fractal dimension increases. We have shown that the mass FD of MCF-7 cells, assessed through the angular light scattering profile, provides an early and sensitive indication of apoptosis. More specifically, in both doxorubicin- and paclitaxel-treated cells the mass FD increases dramatically, with an increase of up to 30% soon after treatment, and remains at an elevated level as the cells undergo apoptosis. Differences for both types of treatment are statistically significant shortly after treatment (1.5−3 hours post-treatment) as well as at later time points, when the cells present more traditional markers of apoptosis induction (12 and 24 hours post-treatment). The fact that statistically significant changes in FD are seen for both treatments indicates that the changes are not drug-specific.

We hypothesized that the mass FD would change as the cells underwent apoptosis due to nuclear fragmentation and/or condensation. Analysis of DAPI-stained images indicated that the box FD did increase to elevated levels at 12 and 24 hours, which could explain the elevated mass FD assessed by a/LCI at those time points. More surprising, and more significant, was the finding of early changes in mass FD, as early as 1.5 hours in 5 nM paclitaxel-treated cells. It is probable that this change occurs due to structural changes in another organelle. Due to the

sensitivity of light scattering to mitochondrial morphology (30,31), we hypothesized that these organelles were largely responsible for the early, and possibly, later observed changes in mass FD. Our analysis of MitoTracker FM Green-stained cells supports this hypothesis. We see significant changes in box FD after 3 hours of treatment with 5 nM of paclitaxel in the mitochondria images. We note that there is an important distinction between computing box FD using fluorescence images and mass FD using a/LCI. Namely, although microscopic imaging is subject to the diffraction limit (~400 nm), a/LCI is sensitive to changes in structure well below the diffraction limit. With this in mind, we acknowledge that there are a number of other organelles that could experience structural changes due to apoptosis-related events soon after treatment. Mass FD would be sensitive to any changes in sub-cellular organization, even those not necessarily detectable by image analysis, provided that the affected organelles undergo topological changes that result in changes in scattered light. However, our data supports the hypothesis that the nucleus and mitochondria are both, at least partly, responsible for the changes in FD.

Two other noteworthy results are the trends in mass FD for both doxorubicin- and 5 nM paclitaxel-treated cells, and the differences in mass FD between 50 nM and 5 nM paclitaxel-treated cells. First, for both 5 nM paclitaxel- and doxorubicin-treated cells, there is an increase in mass FD up to 3 hours, and then a slight reversal at 6 hours followed by a steady increase through 24 hours. Although these trends are not statistically significant, they do manifest in both treatments. The presence of these trends in both treatments lends credence to the possibility that there are at least two distinct mechanisms responsible for the changes in mass FD which occur in two different temporal windows post-treatment. Additionally, the presence of the trend for both apoptosis-inducing treatments indicates that these two distinct mechanisms are inherent to structural changes that occur during, or leading up to, apoptosis. As previously stated, our analysis indicates that mitochondrial structural changes are partly responsible for at least the early changes in mass FD, while nuclear sub-structure changes are at least partly responsible for later changes in mass FD.

The second noteworthy finding was that 50 nM paclitaxel treatment caused early changes in mass FD which then reverted to nearly the mass FD of control cells at later timepoints. The differences between the mass FD of 50 nM paclitaxel-treated cells and control cells are not statistically significant after three hours. This finding is important because the 50 nM paclitaxel treatment did not result in apoptosis within the observation window. This indicates that the early changes seen in mass FD are not necessarily related to apoptosis, but rather to general structural changes in cellular organelles due to events that may lead to apoptosis. For example, mitochondrial changes that occur in response to cellular stress include mitochondrial swelling, and mitochondrial fission and fusion (2,8,9,32). One model of apoptosis suggests that mitochondrial fission is required for and precedes the loss of mitochondrial membrane potential during apoptosis. However, there are reports that inhibition of mitochondrial fission does not block Bax/Bak-dependent apoptosis (32). Our results lend further support to the notion that later changes in FD are related to nuclear fragmentation and apoptosis, but early changes are caused by a different cellular event that may involve mitochondrial fission.

Previous light scattering studies have explored using fractal dimension for detecting apoptosis and dysplasia, but the present study demonstrates stark and statistically significant differences early in treatment, and across multiple treatments. The primary advance that yielded the high degree of sensitivity demonstrated in this study is the use of a T matrix-based ILSA model that accounts for nuclear asphericity. This is in contrast to previous techniques that relied on light scattering model which assumed spherical cell nuclei and organelles. By removing the uncertainty that arises from incompatibility between the shape of the nucleus and the light scattering models previously used in ILSA, we find that the determination of subcellular structures is more accurate and sensitive. Future applications of light scattering can exploit this

increase in sensitivity by employing a T matrix-based ILSA algorithm (or another light scattering model appropriate for nuclear shapes) for assessing mass FD. As a general quantitative assessment of changes in cell structure and organization, mass FD presents a potential new avenue for assessing changes in cell function including differentiation, proliferation, apoptosis, and others.

In conclusion, noninvasive, high-throughput light scattering methods such as a/LCI, are a sensitive indicator of subcellular structure. In the present study, we have used a/LCI to measure fractal dimension of subcellular structures to distinguish between cells treated with apoptosis-inducing drugs and control cells. Moreover, the mass fractal dimension of treated and control cells presents significant differences very soon after treatment. Our studies with image analysis of fluorescently tagged organelles indicates that changes in mitochondrial morphology are partly responsible for early changes in fractal dimension, while changes in nuclear structure are largely responsible for later changes in fractal dimension. These findings suggest that light scattering can be a powerful non-invasive tool for monitoring apoptosis in both basic research experiments and clinical treatments.

Supplementary Material

Refer to Web version on PubMed Central for supplementary material.

Acknowledgements

References

1. Hanahan D, Weinberg RA. The hallmarks of cancer. Cell 2000;100:57–70. [PubMed: 10647931]

2. Taylor RC, Cullen SP, Martin SJ. Apoptosis: controlled demolition at the cellular level. Nat Rev 2008;9:231–41.

3. Blankenberg FG. In vivo detection of apoptosis. J Nucl Med 2008;49(Suppl 2):81S–95S. [PubMed: 18523067]

4. Guo B, Hembruff SL, Villeneuve DJ, Kirwan AF, Parissenti AM. Potent killing of paclitaxel- and doxorubicin-resistant breast cancer cells by calphostin C accompanied by cytoplasmic vacuolization. Breast Cancer Res Treat 2003;82:125–41. [PubMed: 14692656]

5. Saunders DE, Lawrence WD, Christensen C, Wappler NL, Ruan H, Deppe G. Paclitaxel-induced apoptosis in MCF-7 breast-cancer cells. Int J Cancer 1997;70:214–20. [PubMed: 9009163]

6. Krysko DV, Vanden Berghe T, D'Herde K, Vandenabeele P. Apoptosis and necrosis: detection, discrimination and phagocytosis. Methods 2008;44:205–21. [PubMed: 18314051]

7. Kaufmann SH, Lee SH, Meng XW, et al. Apoptosis-associated caspase activation assays. Methods 2008;44:262–72. [PubMed: 18314058]

8. Cereghetti GM, Scorrano L. The many shapes of mitochondrial death. Oncogene 2006;25:4717–24. [PubMed: 16892085]

9. Frank S, Gaume B, Bergmann-Leitner ES, et al. The role of dynamin-related protein 1, a mediator of mitochondrial fission, in apoptosis. Dev Cell 2001;1:515–25. [PubMed: 11703942]

10. Lane JD, Lucocq J, Pryde J, et al. Caspase-mediated cleavage of the stacking protein GRASP65 is required for Golgi fragmentation during apoptosis. J Cell Biol 2002;156:495–509. [PubMed: 11815631]

11. Brown WJ, Pyhtila JW, Terry NG, et al. Review and Recent Development of Angle-Resolved Low-Coherence Interferometry for Detection of Precancerous Cells in Human Esophageal Epithelium. IEEE J. Sel. Top. Quant. Elec 2008;14:88–97.

12. Pyhtila JW, Graf RN, Wax A. Determining nuclear morphology using an improved angle-resolved low coherence interferometry system. Opt Express 2003;11:3473–84.

13. Wax A, Yang CH, Backman V, et al. Cellular organization and substructure measured using angle-resolved low-coherence interferometry. Biophys. J 2002;82:2256–64. [PubMed: 11916880]

14. Krug JT, Wang GD, Emory SR, Nie SM. Efficient Raman enhancement and intermittent light emission observed in single gold nanocrystals. J Am Chem Soc 1999;121:9208–14.

15. Wax A, Yang CH, Muller MG, et al. In situ detection of neoplastic transformation and chemopreventive effects in rat esophagus epithelium using angle-resolved low-coherence interferometry. Cancer Res 2003;63:3556–9. [PubMed: 12839941]

16. Chalut KJ, Kresty LA, Pyhtila JW, et al. In situ assessment of intraepithelial neoplasia in hamster trachea epithelium using angle-resolved low-coherence interferometry. Cancer Epidemiol Biomarkers Prev 2007;16:223–7. [PubMed: 17301253]

17. Chalut KJ, Chen S, Finan JD, Giacomelli MG, Guilak F, Leong KW, Wax A. Label-free, high-throughput measurements of dynamic changes in cell nuclei using angle-resolved low coherence interferometry. Biophys J 2008;94(12):4948–56. [PubMed: 18326642]

18. Levitt JM, Hunter M, Mujat C, McLaughlin-Drubin M, Munger K, Georgakoudi I. Diagnostic cellular organization features extracted from autofluorescence images. Opt Lett 2007;32(22):3305–7. [PubMed: 18026288]

19. Kim YL, Liu Y, Wali RK, et al. Simultaneous measurement of angular and spectral properties of light scattering for characterization of tissue microarchitecture and its alteration in early precancer. IEEE J. Sel. Top. Quant. Elec 2003;9:243–56.

20. Wilson JD, Bigelow CE, Calkins DJ, Foster TH. Light scattering from intact cells reports oxidative-stress-induced mitochondrial swelling. Biophys J 2005;88:2929–38. [PubMed: 15653724]

21. Mulvey CS, Curtis AL, Singh SK, Bigio IJ. Elastic scattering spectroscopy as a diagnostic tool for apoptosis in cell cultures. IEEE J. Sel. Top. Quant. Elec 2007;13:1663–70.

22. Boustany NN, Tsai YC, Pfister B, Joiner WM, Oyler GA, Thakor NV. BCL-x(L)-dependent light scattering by apoptotic cells. Biophys J 2004;87:4163–71. [PubMed: 15377529]

23. Wilson JD, Giesselman BR, Mitra S, Foster TH. Lysosome-damage-induced scattering changes coincide with release of cytochrome c. Opt Lett 2007;32:2517–9. [PubMed: 17767290]

24. Pyhtila JWMH, Simnick AJ, Chilkoti A, Wax A. Analysis of long range correlations due to coherent light scattering from in-vitro cell arrays using angle-resolved low coherence interferometry. J Biomed Opt 2006;11:034022.

25. Mishchenko, MI.; Travis, LD.; Hovenier, JW. Light scattering by nonspherical particles : theory, measurements and applications. Academic; San Diego ; London: 2000.

26. Amoozegar C, Giacomelli MG, Keener JD, Chalut KJ, Wax A. Experimental verification of T matrix based inverse light scattering analysis for assessing structure of spheroids as models of cell nuclei. Appl Opt. 2009under review

27. Giacomelli M, Chalut KJ, Ostrander JH, Wax A. Application of T-matrix method to determine the structure of spheroidal cell nuclei with angle-resolved light scattering. Opt Lett. 2008in press

28. Teixera, J. Experimental methods for studying fractal aggregates.. In: Stanley, HE.; Ostrowsky, N., editors. On Growth and Form, Fractal and Non-Fractal Patterns in Physics. 1986. p. 145-62.

29. Schmitt JM, Kumar G. Turbulent nature of refractive-index variations in biological tissue. Opt Lett 1996;21:1310–2.

30. Boustany NN, Drezek R, Thakor NV. Calcium-induced alterations in mitochondrial morphology quantified in situ with optical scatter imaging. Biophys J 2002;83:1691–700. [PubMed: 12202392]

31. Wilson JD, Foster TH. Mie theory interpretations of light scattering from intact cells. Opt. Lett 2005;30:2442–4. [PubMed: 16196346]

32. Parone PA, James DI, Da Cruz S, et al. Inhibiting the mitochondrial fission machinery does not prevent Bax/Bak-dependent apoptosis. Mol Cell Biol 2006;26:7397–408. [PubMed: 17015472]
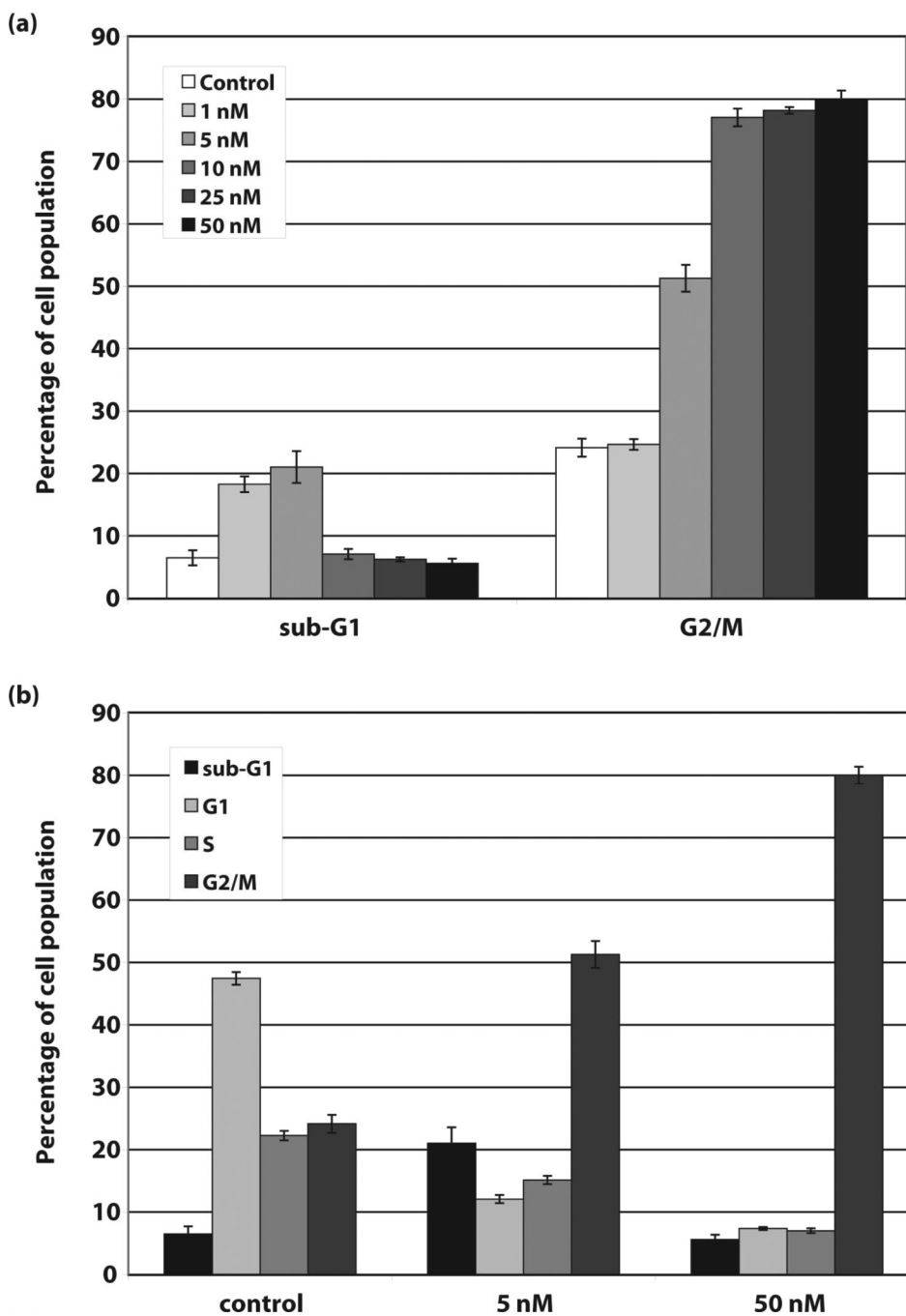
Figure 1. Paclitaxel induces apoptosis and G2/M arrest in MCF-7 breast cancer cells
a) Control MCF-7 cells and cells treated for 24 hours with 1, 5, 10, 25, and 50 nM paclitaxel were fixed and stained with propidium iodide and then analyzed by flow cytometry for cellular DNA content. Results shown in Figure 1a are only the sub-G1 and G2/M (4n) DNA content populations. **b)** Complete cell cycle analysis from control MCF-7 cells and cells treated with 5 nM and 50 nM paclitaxel for 24 hours.
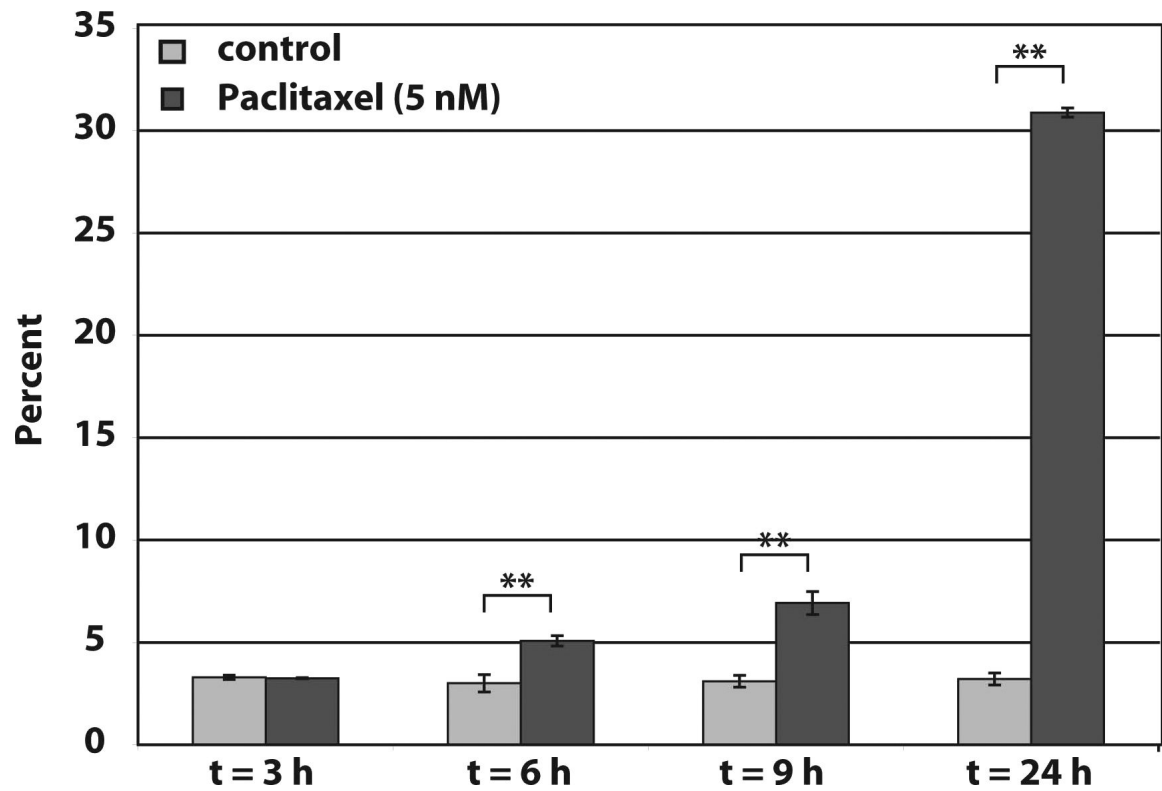
Figure 2. Paclitaxel-treated MCF-7 cells show significant DNA fragmentation within 6
Control and 5 nM paclitaxel-treated MCF-7 cells (3, 6, 9 and 24 hours) were stained with propidium iodide and analyzed by flow cytometry for DNA content, data shown is only the percentage of the cellular population with sub-G1 DNA content. ** indicates high statistical significance ($p < 0.001$).
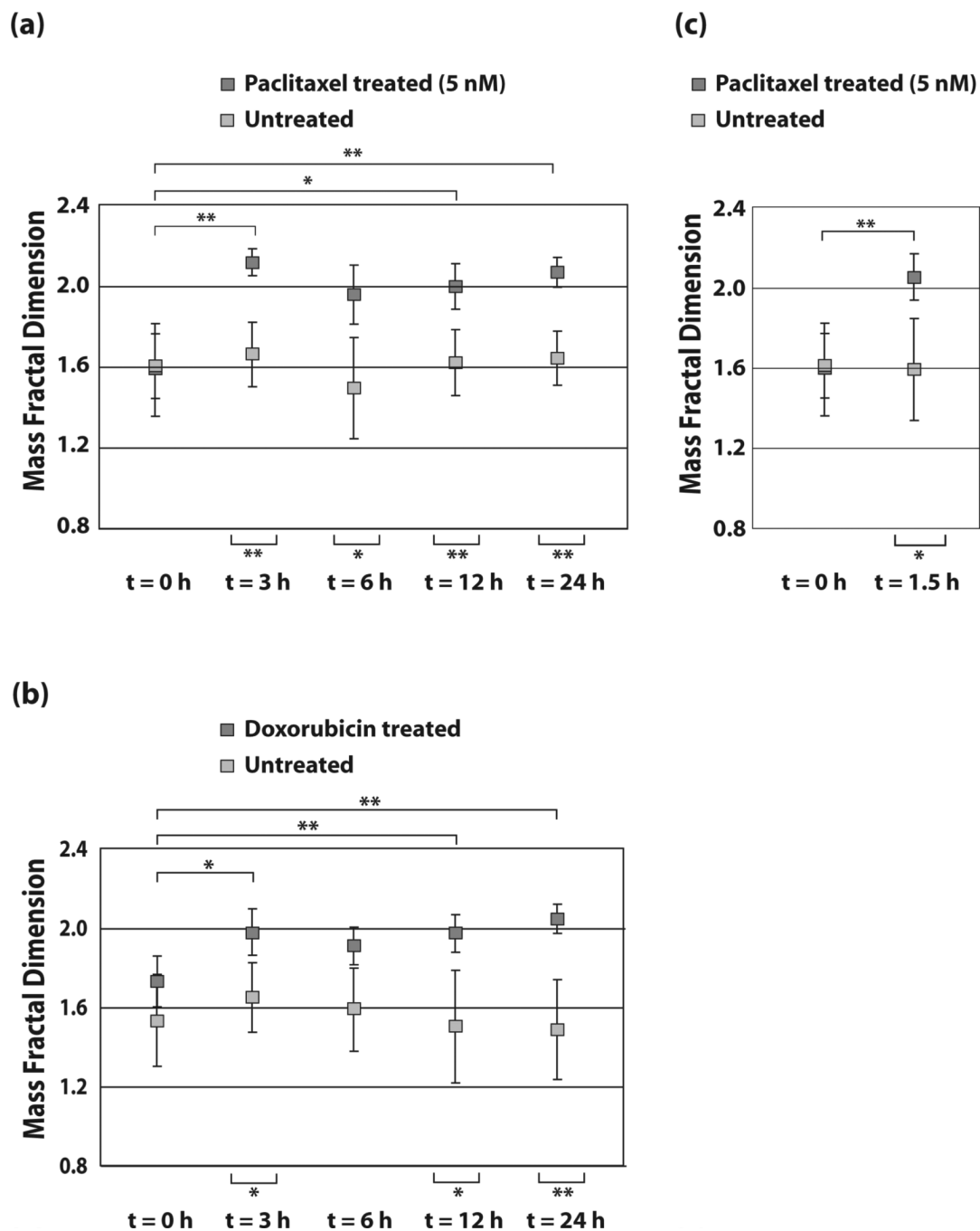
Figure. 3. Paclitaxel and doxorubicin induce a significant change in the mass FD of MCF-7 cells
Summary of mass FD results for MCF-7 cells treated with (a) 5 nM Paclitaxel and (b) 5 μM Doxorubicin at t = 3,6,12 and 24 h post treatment. (c) Comparison of cells treated with 5 nM Paclitaxel and controls at t = 1.5 h. 50 nM Paclitaxel treatment results are shown in supplementary Fig. S3. * indicates statistical significance (p < 0.05) and ** indicates high statistical significance (p < 0.001).
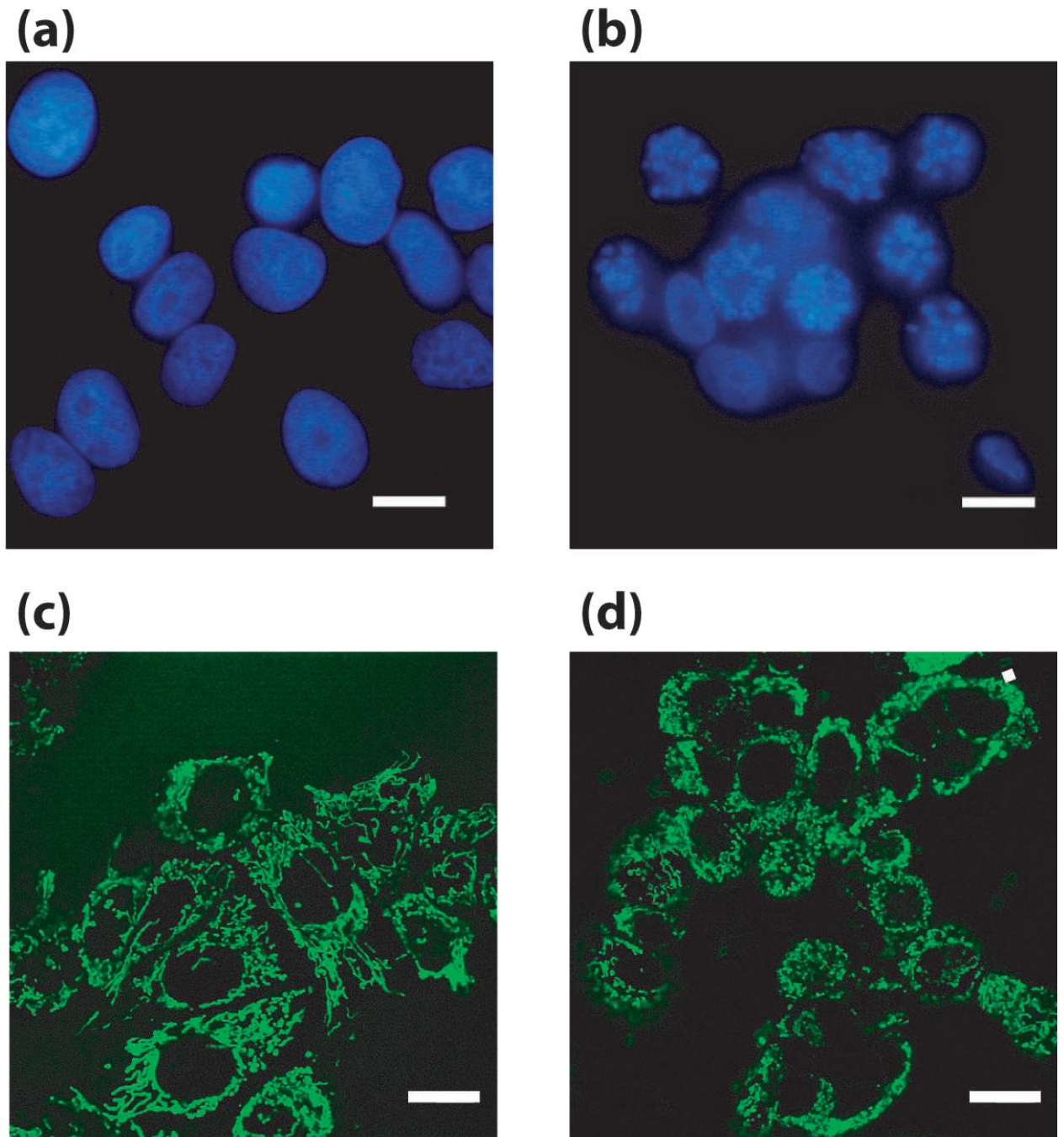
Figure 4. DAPI and MitoTracker images from paclitaxel-treated MCF-7 cells
Representative images from DAPI (a,b) and MitoTracker (c,d) stained control (a,c) and
paclitaxel-treated (b,d) MCF-7 cells Scale bars = 10 μm.
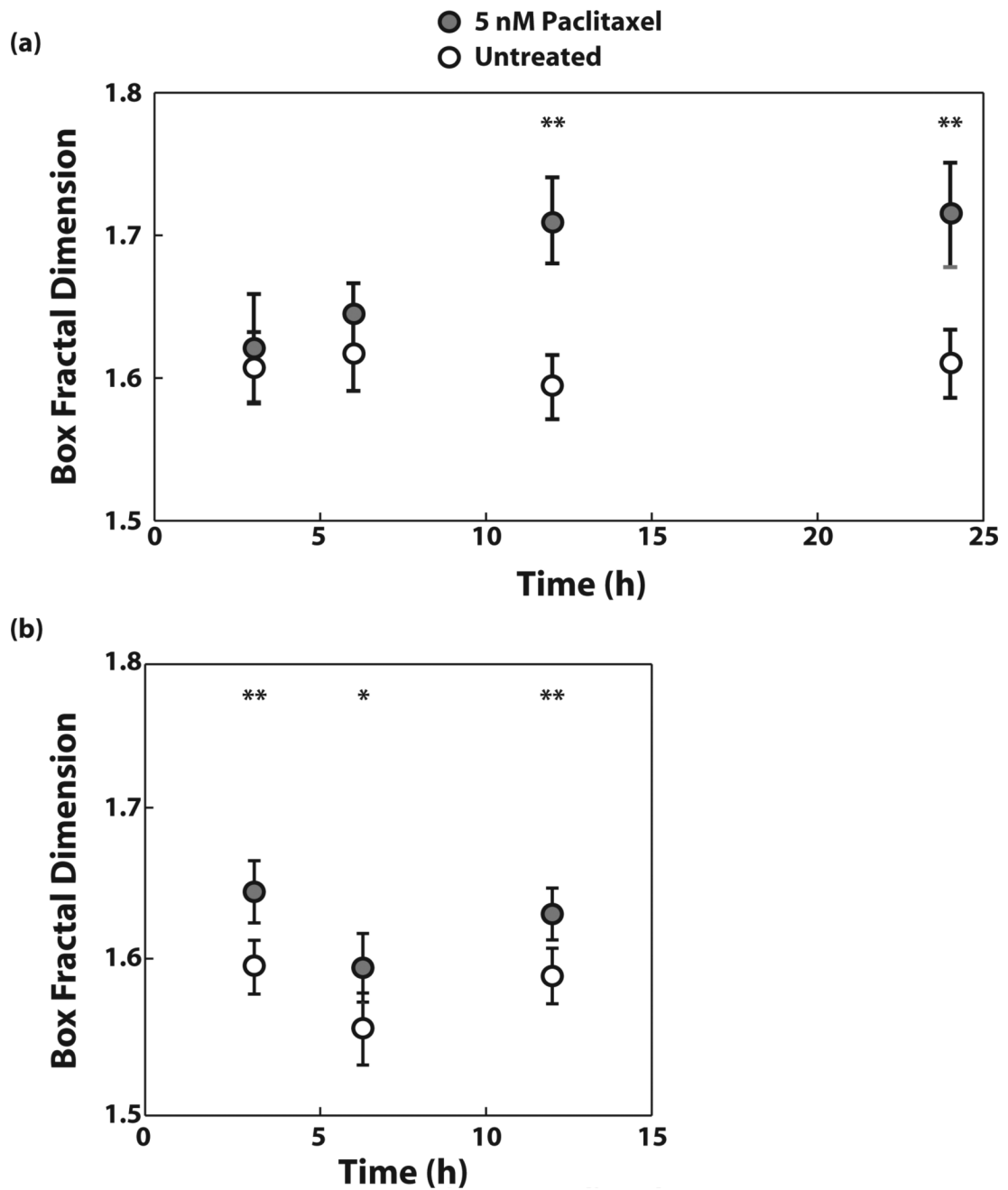
Figure 5. Paclitaxel induces a significant change in the box FD of MCF-7 cell nuclei and mitochondria
(a) nuclei and (b) mitochondria after treatment with 5 nM Paclitaxel for 3, 6, 12, and 24 hours or 3, 6, and 12 hours, respectively. For nuclei, box FD is assessed by QIA of DAPI-stained images using fluorescence microscopy. For mitochondria, box FD is assessed by QIA of MitoTracker FM Green-stained images using confocal fluorescence microscopy.